HHS Public Access

Author manuscript

Nat Immunol. Author manuscript; available in PMC 2019 July 14.

Published in final edited form as:

Nat Immunol. 2019 February ; 20(2): 152–162. doi:10.1038/s41590-018-0287-8.

The Ca^{2+} sensor STIM1 regulates type I interferon response by retaining the signaling adaptor STING at the endoplasmic reticulum

Sonal Srikanth[1,14,15,*], **Jin Seok Woo**[1,14], **Beibei Wu**[1], **Yasser M. El-Sherbiny**[2,3,4], **Jennifer Leung**[1], **Koollawat Chupradit**[5,6,7], **Laura Rice**[8], **Gil Ju Seo**[9], **Guillaume Calmettes**[10], **Chandran Ramakrishna**[11], **Edouard Cantin**[11], **Dong Sung An**[5,6,7], **Ren Sun**[12], **Ting-Ting Wu**[12], **Jae U. Jung**[9], **Sinisa Savic**[2,13], and **Yousang Gwack**[1,15,*]

[1]Department of Physiology, David Geffen School of Medicine, UCLA, Los Angeles, California, USA

[2]National Institute for Health Research—Leeds Biomedical Research Centre and Leeds Institute of Rheumatic and Musculoskeletal Medicine (LIRMM), Wellcome Trust Brenner Building, St James's University Hospital, Beckett Street, Leeds, UK

[3]Clinical Pathology Department, Faculty of Medicine, Mansoura University, Egypt.

[4]School of Science and Technology, Department of Biosciences, Nottingham Trent University, Nottingham, UK

[5]Division of Hematology-Oncology, David Geffen School of Medicine at UCLA, Los Angeles, California, USA

[6]School of Nursing, University of California at Los Angeles, Los Angeles, California, USA

[7]UCLA AIDS Institute, Los Angeles, California, USA

[8]Leeds Institute of Biomedical and Clinical Sciences, University of Leeds, Wellcome Trust Brenner Building, St James's University Hospital, Beckett Street, Leeds, UK

[9]Department of Molecular Microbiology and Immunology, Keck School of Medicine, University of Southern California, Los Angeles, California, USA

[*]Address correspondence to: Dr. Sonal Srikanth or Dr. Yousang Gwack, ssrikanth@mednet.ucla.edu; ygwack@mednet.ucla.edu.

AUTHOR CONTRIBUTIONS

Y.G. and S.S. designed research; S.S. performed all the in vitro experiments using MEFs, THP1 and BMDMs with technical help from J.L.; J.S.W. performed biochemical experiments of interaction between STIM1 and STING, SAVI mutant analyses, and in vivo HSV infection experiments with help from B.W.; Y.M. E.-S, L.R and S.Savic collected and analyzed patient samples together with S.S and J.S.W.; K.C. and D.S.A. performed the HIV infection experiments; G.J.S. and J.U.J. provided reagents and protocols for in vitro HSV infections; G.C. helped with statistical analysis; C. R. and E.C. provided reagents and protocols for in vivo HSV infections; T.T.W. and R.S. provided reagents and protocols for MHV-68 infections; S.S. and Y.G. wrote the manuscript with input from all authors and supervised the project.

COMPETING INTERESTS

The authors do not have any competing financial interests.

Data availability

The data that support the findings of this study are available from the corresponding authors upon request. The manuscript describing clinical phenotype of *STIM1* patient is available from OSR Preprints (https://doi.org/10.31219/osf.io/4duxt).

[10]Department of Medicine (Cardiology), David Geffen School of Medicine at UCLA, Los Angeles, California, USA

[11]Department of Molecular Immunology, City of Hope Beckman Research Institute, Duarte, California, USA

[12]Department of Molecular and Medical Pharmacology, UCLA, Los Angeles, California, USA

[13]Department of Clinical Immunology and Allergy, St James's University Hospital, Leeds, UK

[14]Equal contribution

[15]Senior author

Abstract

STING is an endoplasmic reticulum (ER) signaling adaptor that is essential for the type I Interferon response to DNA pathogens. Aberrant activation of STING is linked to the pathology of autoimmune and autoinflammatory diseases. The rate-limiting step for the activation of STING is its translocation from the ER to the ER–Golgi intermediate compartment. Here we found that deficiency in the Ca^{2+} sensor STIM1 caused spontaneous activation of STING and enhanced expression of type I interferons under resting conditions in mice and a patient suffering from combined immunodeficiency. Mechanistically, STIM1 associated with STING to retain it in the ER membrane, and co-expression of full-length or a STING-interacting fragment of STIM1 suppressed the function of dominant STING mutants that cause autoinflammatory diseases. Furthermore, deficiency in STIM1 strongly enhanced the expression of type I interferons after viral infection and prevented the lethality of infection with a DNA virus in vivo. This work delineates a STIM1–STING circuit that maintains the resting state of the STING pathway.

The endoplasmic reticulum (ER) provides a structural platform for activation of the type I interferon (IFN) response. Stimulator of interferon genes (STING), a key signaling adaptor protein for DNA-sensing pathways localizes to the ER membrane in the resting state[1, 2, 3]. After activation by cytosolic DNAs, it translocates into the ER-Golgi intermediate compartment (ERGIC) to recruit TANK-binding kinase 1 (TBK1) and interferon regulatory factor 3 (IRF3). IRF3, upon phosphorylation by TBK1, homo-dimerizes and translocates into the nucleus to induce transcription of type I IFNs[4, 5, 6, 7]. Beside an essential role in protecting the host against DNA pathogens, STING is also involved in the pathogenesis of autoinflammation caused by self-DNAs in murine models[8, 9]. Accordingly, STING has been implicated in the pathogenesis of Aicardi–Goutieres syndrome (AGS), systemic lupus erythematosus (SLE) and other type I Interferonopathies[10]. Furthermore, mutations in STING have been uncovered in patients with STING-associated vasculopathy with onset in infancy (SAVI) and lupus-like symptoms[11, 12, 13]. The STING variants found in SAVI patients are constitutively active and localize to the ERGIC without the STING ligand, cyclic dinucleotides (CDNs), suggesting that they may escape a mechanism that potentially maintains the ER localization of STING[14]. Since CDNs can be generated by cytosolic self-DNAs derived from mitochondrial damage or genomic instability, and the binding affinity of STING for CDNs is high (~5 nM for 2',3' cyclic guanosine monophosphate-adenosine monophosphate [2',3'-cGAMP])[15], active inhibitory mechanisms are necessary to tightly

control its activation. However, little is known about how the resting state of STING is maintained.

High Ca^{2+} concentration in the ER ($[Ca^{2+}]_{ER}$) is essential for its normal function. At the same time, diverse receptors elevate cytoplasmic $[Ca^{2+}]$ by depleting ER Ca^{2+} stores through a mechanism called store-operated Ca^{2+} entry (SOCE). Stromal interaction molecule 1 (STIM1), an EF-hand-containing Ca^{2+}-binding protein localizes throughout the ER when $[Ca^{2+}]_{ER}$ is high, but after depletion of the ER Ca^{2+} stores, it translocates into junctional areas between the ER and plasma membrane, interacts with the pore subunit of store-operated Ca^{2+} (SOC) channels; Orai1, and induces Ca^{2+} entry[16]. The essential role of STIM1 in effector function of adaptive immune cells including T and B cells has been well established[17, 18, 19]. Mutations in *STIM1* cause severe combined immune deficiency (SCID) in humans[20]. Paradoxically, these patients also suffer from lymphoproliferative and autoimmune complications. Although for some forms of SCID, the mechanisms behind these complications have been worked out; for example, poor development of both central and peripheral tolerance[21], the underlying causes of inflammatory complications in patients harboring mutations in *STIM1* are not unknown.

The role of STIM1 in cells of the innate immune system is currently unclear. Here, we examined the phenotypes of STIM1-deficient cells and observed that loss of STIM1 induces spontaneous activation of the STING-TBK1-IRF3 pathway to activate type I IFN responses under sterile conditions in both murine and human cells. Mechanistically, STIM1 directly interacted with STING to retain it in an inactive state on the ER membrane. Accordingly, we also observed strong resistance to viral infections in STIM1 KO cells and animals. These results suggest that STIM1 plays an important role in regulation of the innate immune responses in addition to its well-established function in regulation of SOCE in adaptive immunity.

Results

STIM1 deficiency induces type I IFN response

To gain insights into possible role of STIM1 in innate immune responses, we checked expression of various inflammatory cytokines in *Stim1*$^{-/-}$ murine embryonic fibroblasts (MEFs). Among these, transcripts of *Ifnb1* and *Il6* as well as interferon-stimulated genes (ISGs) were significantly increased in *Stim1*$^{-/-}$ MEFs compared to those in wild type (WT) cells (Fig. 1a). Accordingly, we observed increased amounts of secreted IFN-β protein in culture supernatants from *Stim1*$^{-/-}$ MEFs (Fig. 1b). Due to the well-established role of STIM1 in SOCE, it was possible that the increased type I IFN response in *Stim1*$^{-/-}$ MEFs was due to altered intracellular Ca^{2+} homeostasis. To check this possibility, we compared responses between *Stim1*$^{-/-}$ and *Orai1*$^{-/-}$ MEFs, both of which show loss of SOCE (Fig. 1c). However, we did not observe enhanced *Ifnb1* expression in *Orai1*$^{-/-}$ MEFs, indicating that block of SOCE or altered intracellular Ca^{2+} levels do not contribute to increased type I IFN response observed in *Stim1*$^{-/-}$ MEFs.

To verify these observations in primary cells, we examined bone marrow-derived macrophages (BMDMs) from WT (*Stim1*$^{fl/fl}$) and *Stim1*$^{fl/fl}$*UBC-ERT2*-cre mice to induce

acute loss of STIM1 expression after tamoxifen treatment (Fig. 1d). Similar to MEFs, we observed enhanced expression of *Ifnb1* and *Il6* transcripts in *Stim1*$^{-/-}$ BMDMs. Next, we examined if this enhanced type I IFN expression phenotype was conserved in human macrophages. We generated *STIM1*$^{-/-}$ THP1 cells by CRISPR/Cas9-mediated genome editing using two different gRNA sequences (Supplementary Fig. 1). Similar to murine cells, we observed an induction of *IFNB1* and *IL6* mRNAs and increased IFN-β secretion in *STIM1*$^{-/-}$ THP1 clones (Fig. 1e, f). Moreover, exogenous expression of STIM1 in these THP1 clones significantly rescued the phenotype by decreasing type I IFN expression. Taken together, these data strongly demonstrate an inhibitory role of STIM1 in type I IFN responses. STIM2 is another member of the STIM family that shares 66% amino acid sequence similarity with STIM1[16]. Both of them are ER-resident proteins, but they function differently in sensing depletion of the ER Ca^{2+} stores and efficacy to activate Orai channels. STIM1 plays a dominant role in activation of SOCE while STIM2 is involved in ER Ca^{2+} homeostasis by sensing subtle changes in $[Ca^{2+}]_{ER}$[2223]. To check a possible function of STIM2 in regulation of type I IFN responses, we generated two independent *STIM2*$^{-/-}$ THP1 clones. However, neither of the STIM2 KO clones showed elevated expression of *IFNB1* transcripts (Supplementary Fig. 2). Collectively, these results establish a specific role for STIM1 in regulating the resting state of the type I IFN responses in murine and human cells.

STING-TBK1-IRF3 pathway links perturbation in STIM1 expression to IFN-β expression

Since both STIM1 and STING, an important regulator for the type I IFN responses, localize to the ER membrane, we checked the possibility that STIM1 regulates the function of STING. Upon activation of STING via exposure to its ligand 2',3'-cGAMP, we observed a pronounced enhancement of *Ifnb1* transcript and protein levels in *Stim1*$^{-/-}$, but not *Orai1*$^{-/-}$ MEFs when compared to those in WT MEFs (Fig. 2a). This higher type I IFN response in *Stim1*$^{-/-}$ MEFs was also observed in the presence of cytosolic DNAs after transfection with IFN stimulatory DNA (ISD) or poly(dA:dT) that are known to activate the STING pathway, but not with poly(I:C), a poor agonist of the STING pathway (Fig. 2b, left). Similarly, we observed elevated transcripts of *IFNB1* in *STIM1*$^{-/-}$ THP1 cells transfected with 2',3'-cGAMP, but not poly(I:C) (Fig. 2b, right).

To determine whether deficiency of STIM1 induces an increase in type I IFN response through the STING-TBK1-IRF3 pathway, we checked for activated IRF3 and TBK1 in WT and *Stim1*$^{-/-}$ MEFs. We examined localization of GFP-IRF3, which was exclusively in the cytoplasm in WT MEFs but showed almost equal distribution in the cytoplasm and nuclei in *Stim1*$^{-/-}$ MEFs (Fig. 2c). Biochemically, we detected enhanced homo-dimers of IRF3, in *Stim1*$^{-/-}$ MEFs compared to WT cells under resting conditions (Fig. 2d). Furthermore, we found enhanced levels of phosphorylated TBK1 and accordingly increased ratio of p-TBK1 vs. total TBK1 in *Stim1*$^{-/-}$ MEFs, BMDMs and *STIM1*$^{-/-}$ THP1 cells (Fig. 2e). We could also detect enhanced dimerization of endogenous STING in *Stim1*$^{-/-}$ MEFs, which is considered an active form of STING (Supplementary Fig. 3a). Likewise, *STIM1*$^{-/-}$ HEK293T cells stably expressing STING also showed enhanced STING dimers and multimers (Supplementary Fig. 3b). Next, we examined whether co-deletion of STING in STIM1-deficient cells could rescue this enhanced IFN-β expression phenotype. Deletion of

both *Stim1* and *Tmem173* (gene encoding STING) in MEFs (double knockout, DKO) dramatically reduced *Ifnb1* and *Il6* transcripts under resting or cGAMP-treated conditions (Fig. 2f). Co-deletion of *Tmem173* also rescued increased IFN-β secretion observed in *Stim1*$^{-/-}$ MEFs treated with poly (dA:dT) (Fig. 2g). We observed very similar results using THP1 cells. Deletion of both *STIM1* and *TMEM173* in double knockout (DKO) THP1 cells was confirmed by immunoblotting and SOCE measurements (Fig. 2h). DKO THP1 cells showed reduced *IFNB1* and *IL6* mRNA levels, suggesting that the elevated cytokine expression in *STIM1*$^{-/-}$ THP1 cells were derived from increased STING activity. Together, these results suggest that the increase in type I IFN responses observed in STIM1-deficient cells is mediated by the STING-TBK1-IRF3 pathway, and STIM1 plays a novel role in type I IFN signaling via regulating STING function.

Increased type I IFN responses in patient lacking STIM1 expression

Previously, patients showing SCID symptoms and bearing homozygous nonsense mutation of STIM1 (E136X) were shown to lack STIM1 expression due to nonsense-mediated mRNA decay[24]. To mimic the phenotype of this patient, we transduced STIM1-deficient cells with viral vectors encoding WT and STIM1^{E136X} proteins. We confirmed lack of STIM1 expression in *Stim1*$^{-/-}$ MEFs transduced to express STIM1^{E136X} while those with STIM1^{WT} showed expression similar to the endogenous protein in WT MEFs (Fig. 3a). Importantly, expression of STIM1^{WT} but not STIM1^{E136X} rescued the increased type I IFN response in *Stim1*$^{-/-}$ MEFs (Fig. 3b).

To examine if this was true in STIM1-deficient patients, we harvested primary cells from a patient lacking STIM1 expression due to a homozygous *STIM1* mutation c.478del, p.(Ser160fs). The lack of STIM1 expression in patient's PBMCs was confirmed by immunoblotting (Fig. 3c). Patient serum showed enhanced IFN-β, IL-6 and TNF cytokines when compared to those observed in three healthy controls (Fig. 3d). Consistently, we also observed enhanced expression of ISGs in PBMCs and monocytes from the patient, when compared to those in two healthy controls (Fig. 3e). Interestingly, the patient also exhibited very mild SAVI-like symptoms – he suffered from desquamation and blistering with skin eruptions mainly affecting the palm, soles of the feet and cheeks. He also showed pronounced nail dystrophy[25]. Together, these data confirm that loss of STIM1 in humans enhances expression of type I IFN, proinflammatory cytokines and ISGs, similar to murine cells.

STIM1 interacts with STING for its retention at the endoplasmic reticulum

The increased type I IFN response together with higher basal activity of the STING-TBK1-IRF3 pathway in STIM1-deficient cells suggests that STIM1 may be involved in maintaining the resting state of the STING pathway. Microscopy analysis showed a strong co-localization between STIM1 and STING in the ER (Fig. 4a). Hence, we checked if STIM1 can physically interact with STING to retain it in the ER. When co-expressed in HEK293T cells, STIM1 was specifically identified from immunoprecipitates of STING (Fig. 4b). In addition, we also validated association between endogenous STIM1 and STING proteins by immunoprecipitation (Fig. 4c). This association was specific because another ER-resident protein, calnexin could not be detected in immunoprecipitates of STIM1.

Next, we examined association between STIM1 and STING upon activation of either of the proteins. We activated STIM1 by treatment with thapsigargin that depletes the ER Ca^{2+} stores, and activated STING using its ligand, 2',3'-cGAMP. We observed reduced biochemical association between the two proteins by stimulation of either STIM1 or STING (Fig. 4d). These data indicate that STING and STIM1 form a protein complex that is dissociated due to conformational changes induced by stimulation of either of these proteins. Association between STING and STIM1 prompted us to check for a possible role of STING in regulating the function of STIM1. We observed reduced SOCE induced by thapsigargin or anti-CD3 antibody treatment in HEK293T and Jurkat T cells overexpressing STING (Supplementary Fig. 4a, b, c). In addition, we observed enhanced STIM1 translocation to the ER-PM junctions in thapsigargin treated STING-deficient (*Tmem173*$^{-/-}$) MEFs (Supplementary Fig. 4d). Conversely, there was significant enhancement of SOCE in *TMEM173*$^{-/-}$ Jurkat cells (Supplementary Fig. 4e, f). This enhancement was not observed in THP1 cells, indicating cell type specificity (Fig. 2h). Taken together, these data show that association with STING impacts the function of STIM1 in mediating SOCE.

STING contains four transmembrane (TM) segments in its N terminus that span the ER membrane (Fig. 4e)[1]. STING N-terminal domain (NTD) containing the TM segments plays an important role in its ER localization, trafficking and interaction with regulators including ZDHHC1, AMFR, TRIM32, and RNF5[26, 27, 28, 29]. Tumor DNA viral proteins, E1A and E7 also bind to STING NTD to inhibit downstream signaling[28]. The cytoplasmic region (C-terminal domain, CTD) of STING contains the dimerization domain (DD), CDN-binding region, and the C-terminal tail (CTT) that interacts with TBK1 and IRF3. STIM1 has an N-terminal ER-luminal region containing the Ca^{2+}-sensing EF-hand motifs and sterile alpha motif (SAM) domain that is important for its multimerization after ER Ca^{2+} depletion. It also has a single TM domain that traverses the ER membrane. The cytoplasmic C terminus contains multiple functional domains including coiled-coil domains (CC) 1, CC2, CC3, a serine/threonine-rich domain (S/T), and a lysine-rich domain (poly-K) that are important for binding to the plasma membrane after depletion of ER Ca^{2+} stores. A fragment containing CC2 and CC3 of STIM1 called the CRAC activation domain (CAD) or the STIM1 Orai activating region (SOAR) was identified to interact directly with Orai1 subunits to gate them[16, 29].

To determine their interaction domains, we carried out co-immunoprecipitation using lysates of HEK293T cells overexpressing full-length, NTD or CTD of STING together with full-length STIM1. These results showed NTD of STING as a major STIM1-interacting domain while its CTD interacted weakly with STIM1 (Fig. 4f, left panels). To uncover the domain(s) of STIM1 involved in interaction with STING, we performed GST pull-down experiments by incubating bacterially purified GST-fused fragments of STIM1 with lysates of HEK293T cells overexpressing full-length, NTD or CTD of STING. From this analysis, we identified a predominant interaction between the N terminus of STIM1 containing the TM segment (a.a. 1–249) and STING NTD, and a weaker binding of the cytoplasmic fragment predominantly containing the S/T-rich region of STIM1 to STING CTD (Fig. 4f, right panels). These data suggest that interaction between STIM1 and STING is predominantly mediated by their TM domains on the ER membrane with weak additional interactions between their cytoplasmic regions.

STIM1 acts as an ER retention factor to suppress the activity of STING

Ligand binding induces conformational rearrangement and trafficking of STING from the ER to the ERGIC and the Golgi apparatus[14, 30, 31]. Since STIM1 interacted strongly with STING NTD, which is crucial for STING localization, we hypothesized that STIM1 may control the ER localization of STING. To validate this hypothesis, we examined the localization of STING in WT and *Stim1*$^{-/-}$ MEFs by co-staining with ERGIC marker (ERGIC-53/p58). We observed a significant population of *Stim1*$^{-/-}$ MEFs showing partial localization of STING at the ERGIC without any stimulation, and this population increased much faster in *Stim1*$^{-/-}$ MEFs infected with the DNA virus, herpes simplex virus type-1 (HSV-1) when compared to WT MEFs (Fig. 5a). To check how interaction with STIM1 influences the function of STING, we monitored the translocation kinetics of STING after treatment of WT or *Stim1*$^{-/-}$ MEFs with 2',3'-cGAMP and observed faster translocation of STING into the ERGIC in *Stim1*$^{-/-}$ MEFs than in WT cells (Fig. 5b). Together with our biochemical analysis, these data suggest that STIM1 physically interacts with STING to promote its retention onto the ER membrane.

We checked if overexpression of STIM1 can inhibit the function of STING using *Ifnb* promoter-driven luciferase reporter (IFN-Luc) assays after 2',3'-cGAMP treatment. In cells co-expressing STING and increasing amounts of full length or the N- and C-terminal binding fragments of STIM1, we observed a dose-dependent inhibition of luciferase reporter expression (Fig. 5c). In support of our biochemical analyses, the N-terminal TM-containing fragment of STIM1 (a.a. 1–249) showed a stronger inhibition of luciferase reporter activity than the cytoplasmic domain (a.a. 400–600) while STIM1 fragments (a.a. 250–400 and a.a. 600–685) that do not interact with STING did not affect luciferase activity. Of note, expression of full-length STIM1 or its N-terminal fragment (a.a. 1–249) did not influence the luciferase activity when stimulated with poly(I:C). These data validate functional interaction between STIM1 and STING proteins.

The genetic lesions of patients exhibiting autoinflammatory vasculopathy and autoimmunity were mapped to single amino acid substitutions in STING[11]. These substitution mutations changed one of the conserved residues V147, N154, or V155, all of which are localized in or around the STING dimerization domain[32]. In addition, these substitutions lead to localization of STING at the ERGIC and constitutive TBK1 and IRF3 activation and uncontrolled type I IFN response[11, 13]. We examined if these disease-associated STING mutants retained binding to STIM1. Using immunoprecipitation analysis, we observed reduced interaction of the STING SAVI mutants with STIM1 and overexpression of full-length or N-terminal fragment of STIM1 could suppress *Ifnb* promoter-driven luciferase activity of these mutants. (Supplementary Fig. 5a, b). In support of these data, confocal analyses showed a partial block of constitutive ERGIC localization of these mutants in the presence of STIM1 (Supplementary Fig. 5c). Collectively, these results confirm the previous observations that exit from the ER is an important step for the activation of STING and STIM1 can block this trafficking via direct interaction.

Genetic inhibition of STIM1 expression primes antiviral activity

We sought to determine whether deficiency of STIM1 influences activation of the type I IFNs in response to DNA virus infection. To examine this, WT and *Stim1*$^{-/-}$ MEFs were infected with DNA viruses (e.g., HSV-1 and murine γ-herpesvirus, MHV-68). Spontaneous induction of IFN-β observed in *Stim1*$^{-/-}$ MEFs was substantially increased after HSV-1 infection (Fig. 6a). We also observed a marked reduction in expression of GFP, encoded from the viral genome which served as an indicator for viral replication in *Stim1*$^{-/-}$ MEFs. We observed similar results using another DNA virus, MHV-68. Similar to HSV-1 infection, MHV-68-infected *Stim1*$^{-/-}$ MEFs showed much lower expression of the viral genome-driven GFP, as well as early and late phase viral transcripts (e.g., *ORF57* and *ORF29*, respectively), indicative of a lower viral burden (Fig. 6b). In consistence with these data, *Stim1*$^{-/-}$ MEFs showed enhanced phosphorylation of IRF3 upon HSV-1 infection (Fig. 6c). We observed similar results in primary cells, where *Stim1*$^{-/-}$ BMDMs showed enhanced expression of *Ifnb1* and *Il6* mRNAs under resting conditions, as well as after HSV-1 infection (Fig. 6d). Together, these data show that loss of STIM1 increases resistance to DNA virus infections.

Next, we validated these observations in *STIM1*$^{-/-}$ THP1 macrophages. Similar to data with mouse cells, STIM1 deficiency rendered human macrophages resistant to HSV-1, decreasing expression of GFP as observed by microscopy and transcript analyses (Fig. 6e). Accordingly, we observed enhanced expression of *IFNB1* transcripts in *STIM1*$^{-/-}$ THP1 cells. Previously, it was shown that anti-viral immunity against HIV infection also relies on the cGAS-STING pathway due to the presence of cytosolic DNA generated by reverse-transcription[8, 33]. To investigate whether STIM1 deletion imparts resistance to HIV, we infected wild type and *STIM1*$^{-/-}$ THP1 cells with GFP-HIV and observed a dramatic reduction of HIV infection in *STIM1*$^{-/-}$ THP1 cells as judged by frequency of GFP^{+} cells (Fig. 6f). Together, these results suggest that deficiency of STIM1 can prime host response against infection with DNA viruses and retroviruses in various murine and human cell types.

Many DNA viruses, including HSV-1 are known to activate Ca^{2+} signaling for a productive infection[34]. Hence it is possible that resistance to DNA virus infection in *Stim1*$^{-/-}$ MEFs may be due to loss of SOCE. To determine the contribution of SOCE versus enhanced STING activity in host resistance to DNA virus infection, we compared responses of *Stim1*$^{-/-}$ and *Orai1*$^{-/-}$ MEFs to HSV-1 infection. We observed a moderate resistance to HSV-1 infection in *Orai1*$^{-/-}$ MEFs, but in comparison, the resistance to HSV-1 infection was approximately 100-fold more pronounced in *Stim1*$^{-/-}$ cells (Supplementary Fig. 6a). In support of the SOCE-independent role of STIM1 in regulation of STING function, we found that *Ifnb1* mRNA expression was not increased after HSV-1 infection in *Orai1*$^{-/-}$ cells contrary to *Stim1*$^{-/-}$ cells. Finally, *Stim1*$^{-/-}$ MEFs when treated with inhibitor of the IFN receptor-JAK-STAT pathway, tofacitinib, became susceptible to HSV-1 infection (Supplementary Fig. 6b). Together, these results indicate a predominant role of the type I IFN pathway in the resistance of STIM1-deficient cells to viral infections.

Ablation of STIM1 primes type I IFN response in vivo

To gain insight into the importance of STIM1 in host defense against viral infection in vivo, we investigated the antiviral immune response in *Stim1*$^{fl/fl}$ and *Stim1*$^{fl/fl}$*Lyz2*-cre mice. In parallel, to compare the contribution of SOCE in host resistance to viral infections, we generated conditionally targeted Orai1 animals (Supplementary Fig. 7a), which were bred with *Lyz2*-cre for two generations. BMDMs differentiated from bone marrows of *Orai1*$^{fl/fl}$*Lyz2*-cre animals showed almost a complete loss of Orai1 transcripts and SOCE (Supplementary Fig. 7b, c). Since HSV-1 is a neurotropic virus and the leading cause of sporadic viral encephalitis, we investigated the effects of *Orai1* and *Stim1* deficiency on HSV-1-induced lethality and viral loads in the brain. When infected with HSV-1 intravenously, control (*Stim1*$^{fl/fl}$ and *Orai1*$^{fl/fl}$) as well as *Orai1*$^{fl/fl}$*Lyz2*-cre animals showed susceptibility and died within 6–8 days of infection (Fig. 7a, b). In contrast *Stim1*$^{fl/fl}$*Lyz2*-cre mice were completely resistant to HSV-1-induced lethality, and accordingly, recovered from loss of body weight. Viral titers in the brains obtained from *Stim1*$^{fl/fl}$*Lyz2*-cre mice were significantly lower than *Stim1*$^{fl/fl}$ animals (Fig. 7c). Importantly, serum cytokine measurements showed elevated levels of serum IFN-β, IL-6 and TNF in uninfected as well as HSV-1-infected *Stim1*$^{fl/fl}$*Lyz2*-cre mice, when compared to littermate controls (Fig. 7d). Taken together, our data indicate that genetic deletion of *Stim1* but not *Orai1* can impart protection from HSV-induced encephalitis and lethality, due to pre-activation of the STING-mediated type I IFN signaling pathway.

Discussion

STING and STIM1 commonly contain transmembrane domain(s) in their N termini and predominantly localize to the ER membrane. Co-immunoprecipitation experiments showed an association between the two proteins, that was primarily mediated by their N-terminal transmembrane domains. We showed that loss of STIM1 renders cells and mice strongly resistant to viral infections due to enhanced expression of type I IFNs and pro-inflammatory cytokines. Importantly, a patient with a mutation in *STIM1* that abrogated STIM1 expression also showed elevated cytokines and ISGs. Furthermore, some of the patient's clinical features, principally the skin and nail manifestations resemble that of SAVI patients, suggesting that the excessive type I IFNs do have adverse biological manifestation in this condition[25]. Mechanistically, enhanced translocation and dimerization of STING by STIM1 deficiency suggest that STIM1 may preferentially bind to STING monomers at the ER to prevent its spontaneous activation. Conversely, we also found that STING deficiency augmented translocation of STIM1 and Ca^{2+} entry triggered by depletion of ER Ca^{2+} stores. Therefore, our studies suggest that physical and functional association between STIM1 and STING is crucial for maintenance of the resting state of both pathways.

We showed that enhanced type I IFN expression in STIM1-deficient cells is not mediated by Ca^{2+} signaling by comparative studies with Orai1-deficient cells and animals. STIM1 deficiency made cells and mice strongly resistant to HSV-1 infections. Since many viruses including HSV-1[34], require elevated Ca^{2+} levels for their replication, we determined the contribution of the Ca^{2+}-dependent (i.e., decreased SOCE) vs. Ca^{2+}-independent mechanisms (i.e., enhanced type I IFN response) involved in anti-viral immunity in STIM1-

deficient cells using two independent molecular tools, *Orai1*$^{-/-}$ cells/mice and JAK inhibitors. These results suggest that decreased viral burden in STIM1-deficient cells and mice is predominantly derived from enhanced type I IFN responses. Whether the same principle can be applied to other viruses with various degrees of dependence on Ca^{2+} signaling and activation of the STING pathway needs further studies.

Although much is understood regarding the mechanisms underlying activation of STING including ligand binding, trafficking and interaction with downstream effector molecules, little is known about regulation of its resting state. Multiple mechanisms underlying STING inhibition have been uncovered due to the importance of timely inactivation of the type I IFN signaling pathway. NLRX1 and ATG9a have been shown to inhibit STING-TBK1 interaction[26, 27]. In addition, K48-linked polyubiquitination by RNF5 and TRIM30a results in STING degradation after ligand binding[35, 36]. All these inhibitory mechanisms target STING function after ligand binding and trafficking. However, inhibition of STING trafficking by brefeldin A, an inhibitor of ADP ribosylation factor (ARF) GTPases, blocks activation of the downstream pathway, suggesting that trafficking of STING is crucial for its function[14]. Consistently, our studies reveal a novel mechanism of regulation of STING activity, inhibition of STING trafficking via direct interaction with STIM1. Activity of three of the disease-associated STING variants; V147L, N154S, and V155M was suppressed by STIM1 in part via blocking their translocation to the ERGIC, demonstrating a therapeutic potential of our finding. In summary, our study identifies STIM1 as an “ER retention factor” to maintain ER residency and inactive conformation of STING. Further, it suggests that one of the primary functions of CDN binding to STING is to disrupt its association with STIM1 that would allow exit of STING from the ER. Further dissection of the mechanisms underlying maintenance of the resting state of STING may inform the design of specific therapeutic strategies geared towards enhancement/inhibition of STING activity in the context of vaccination and sterile inflammatory diseases (e.g., AGS and SAVI), respectively.

Methods

Chemicals and Antibodies.

Fura 2-AM (F1221) was purchased from ThermoFisher Scientific. Thapsigargin and ionomycin were purchased from EMD Millipore. Poly(I:C) (P1530) was purchased from Millipore Sigma. Poly(dA:dT) (tlrl-patn) and 2’,3’-cGAMP (tlrl-nacga23) were purchased from InvivoGen. Tofacitinib (S500110MG) was purchased from Selleck Chemical LLC. Antibodies for detection of STIM1 (5668S), phosphor-IRF3 (29047S), IRF3 (4302S), phosphor-TBK1 (5483S), total TBK1 (3504S), STING (13647S), 6xHis tag (12698S), and STIM2 (4917S) were purchased from Cell Signaling Technologies. Antibodies for detection of FLAG tag (F3040), p58 (ERGIC marker, E1031) and human Orai1 (AB9868) were purchased from Millipore Sigma. Antibody for detection of β-actin (sc-47778) was obtained from Santa Cruz Biotechnology and antibodies for detection of STIM1 (clone 5A2) and GAPDH (GTX100118) from human PBMCs were obtained from Sigma and GeneTex respectively.

Plasmids and cells.

STIM1-YFP plasmid has been described previously[37]. Human STIM1 cDNA was subcloned into a lentiviral vector, FGIlF (kind gift from Dr. Dong Sun An, UCLA) with a C-terminal FLAG tag and pcDNA 3.1 mychis plasmid. GST-tagged truncated fragments of STIM1 corresponding to amino acids 1–249 (containing the EF-hand, SAM domain and transmembrane segment), 250–400 (containing coiled-coil domains 1 and 2), the CAD domain (amino acids 342–448), 400–600 (the serine and threonine-rich region), and 600–685 (the C-terminal PIP_2-interacting domain) have been previously described[37]. Fragments of STING corresponding to the N-terminal TM domain (a.a. 1–154) and C-terminal domain (a.a. 149–379), both tagged with a FLAG tag in the C-terminus, were subcloned into pMSCV-CITE-eGFP-PGK-Puro vector. Full-length cDNA of human STING and SAVI mutants corresponding to V147L, N154S and V155M were subcloned into pEGFPN1 vector to generate a C-terminal GFP fusion protein and into pMSCV-CITE-eGFP-PGK-Puro vector that encodes a C-terminal FLAG tag using primers described in Supplementary Table 1. Oligonucleotides encoding sgRNAs to delete *STIM1*, *STIM2* and *STING* were subcloned into lentiGuide-Puro vector (Addgene, #52963). HEK293T, Vero and Jurkat E6–1 T cell lines were obtained from American Type Culture Collection center (ATCC, Manassas, VA). WT and $Stim1^{-/-}$ MEFs were generated by breeding $Stim1^{fl/fl}$ mice (Jackson Laboratory, stock No. 023350) with *CMV*-cre mice (Jackson Laboratory, stock No. 006054). MEFs were established using standard protocols from E14.5 embryos and retrovirally transduced with SV40 large T antigen in a plasmid encoding hygromycin resistance for immortalization. $Orai1^{-/-}$ MEFs have been previously described[38].

Cell Culture.

MEFs, Vero and HEK293T cells were grown in complete DMEM (Mediatech) supplemented with 10% (v/v) fetal bovine serum (Hyclone), 2 mM L-glutamine (Mediatech), 10 mM HEPES (Mediatech) and Penicillin/Streptomycin (Mediatech) at 37°C and 5% CO_2. BMDMs were differentiated from bone marrow cells isolated from femur and tibia of 6–8-week-old mice. For preparation of BMDMs, the bone marrow cells were cultured in 10% M-CSF-containing conditional medium from HEK293T cells expressing recombinant M-CSF (a kind gift from Stephen Smale lab, UCLA) for 4–6 days. BMDMs were cultured in the absence of M-CSF for at least 24 hours prior to experimental use. THP1 and Jurkat T cells were cultured in RPMI (Mediatech) containing 10% fetal bovine serum (Hyclone). Cells were infected with indicated MOIs of indicated viruses and harvested in TRIzol Reagent for transcript expression analysis. For 2',3'-cGAMP treatment, MEFs or HEK293T cells were treated with or without 1 μM 2',3'-cGAMP for 30 mins in digitonin permeabilization buffer (50 mM HEPES, 100 mM KCl, 3 mM $MgCl_2$, 0.1 mM DTT, 85 mM sucrose, 0.2% BSA, 1 mM ATP, 0.1 mM GTP, pH 7.0) followed by culture medium for indicated times, after which the cells were harvested for transcript analysis or reporter assays. MEFs were transfected with 5 μg of interferon stimulatory DNA (ISD[39]), polydA:dT or poly I:C using Lipofectamine 2000 (Thermofisher Scientific). For ELISAs, MEFs were treated with cGAMP as described and supernatant harvested after 24 hrs.

Mice.

Stim1$^{fl/fl}$ animals were purchased from Jackson Laboratory (stock No. 023350) and bred with *Lyz2*-cre animals (Jackson Laboratory, stock No. 004781) for two generations. Targeting of murine *Orai1* was performed by flanking exon 2 with LoxP sites by homologous recombination in AB2.2 (129SvEv) embryonic stem (ES) cells. Exon 2 encodes for 201 a.a. out of a total of 304 a.a. of Orai1 protein. G418-resistant clones were screened by PCR for homologous recombination at both homology arms. Chimeric mice with floxed *Orai1* alleles were generated by blastocyst injection of heterozygous *Orai1*$^{fl/+}$ ES cell clones. Founder *Orai1*$^{fl/+}$ mice were bred with Flp-deleter mice (Jackson Laboratory) to remove the neomycin resistance gene cassette. *Orai1*$^{fl/fl}$ mice were backcrossed to C57/BL6/J mice for at least 10 generations and then bred with *Lyz2*-cre mice to generate myeloid-specific deletion of *Orai1*. All mice were maintained in pathogen-free barrier facilities and used in accordance with protocols approved by the Institutional Animal Care and Use Committee at the UCLA.

Patient.

Sample collection from the patient was performed after obtaining written consent from his parents according to the principles of the Declaration of Helsinki and after local ethics approval. Detailed clinical evaluation was undertaken in appropriate clinical setting. PBMC isolation from healthy control and patient human blood samples was performed by gradient separation using Lymphoprep (Stem Cell Technologies). Monocytes were purified from PBMCs using a Monocytes separation kit II (# 130-091-153, Miltenyi Biotec). The patient is a 4-year-old boy of consanguineous Pakistani background, who initially presented to paediatric neurology due to poor mobility. A diagnosis of STIM1 deficiency was made following referral to paediatric immunology due to recurrent sinopulmonary infections. The patient has typical non-immunological features consistent with STIM1 deficiency including amelogenesis imperfecta resulting in complete dental clearance, anhidrosis and muscle weakness. Surprisingly, the patient had mild immunodeficiency phenotype, with relatively preserved immunological function, including appropriate responses to challenge vaccination[25].

Virus amplification and concentration.

MHV68-GFP virus was amplified and titrated in NIH3T3 cells using standard protocols. HSV-1 KOS strain was used for all in vitro experiments and HSV-1 17+ strain was used for in vivo infection experiments. Both the strains were amplified and titrated in Vero cells using standard protocols. HSV-1 17+ strain was concentrated for in vivo experiments. VSV-G pseudotyped HIV-1_{NL4-3} strain-GFP reporter virus was amplified and titrated in HEK293T cells using standard protocols.

RNA isolation, cDNA synthesis and Real-time quantitative PCR.

Total RNA from cells harvested in TRIzol Reagent (ThermoFisher) was isolated using the Direct-zol RNA isolation kit (Zymo Research). RNA quantity and quality were confirmed with a NanoDrop ND-1000 spectrophotometer. cDNA was synthesized using 2–3 μg of total RNA using oligo(dT) primers and Maxima Reverse Transcriptase (Thermofisher Scientific).

Real-time quantitative PCR was performed using iTaq Universal SYBR Green Supermix (Bio-Rad) and an iCycler IQ5 system (Bio-Rad) using gene-specific primers described in Supplementary Table 1. Threshold cycles (C_T) for all the candidate genes were normalized to those for *36b4* to obtain ΔC_T and further normalized to the values obtained for WT samples to obtain $\Delta\Delta C_T$. The specificity of primers was examined by melt-curve analysis and agarose gel electrophoresis of PCR products. Total RNA from human patient and healthy donors PBMCs and monocytes harvested was isolated using the Total RNA purification Kit (Norgen Biotek Corp.). cDNA was synthesized using 1–2 μg of total RNA using High-Capacity cDNA Reverse Transcription Kit (ThermoFisher Scientific). Real-time quantitative PCR was performed using TaqMan Universal PCR Master Mix (ThermoFisher Scientific) using FAM-MGB probes for detection of *MX1* (Hs00895608_m1), *IFI44* (Hs00951349), *IFI44L* (Hs00915292_m1), *IFI27* (Hs01086370_m1), *ISG15* (Hs00192713_m1), *CXCL10* (Hs01124251_g1), *RSAD2* (Hs01057264_m1), *IFIT1* (Hs01675197_m1), *IFI6* (Hs00242571_m1), *OAS1* (Hs00973635_m1), *IL6* (Hs00985639_m1), and *HPRT1* (Hs99999909_m1). The relative abundance of each transcript was normalized to the expression level of *HPRT1* to obtain ΔC_T and further normalized to the values obtained for healthy controls to obtain $\Delta\Delta C_T$.

Cytokine measurement by ELISA.

ELISA was performed on cell culture supernatants from indicated cells or serum samples harvested from mock or HSV-1-infected animals for detection of IFNβ (Biolegend, # 439407), IL-6 (ThermoFisher, # 88-7064-88) and TNF (ThermoFisher, # 88-7324-88). Serum samples obtained from healthy controls or STIM1-deficient human patient were used for detection of IFNβ (PBL Assay Science, #41410), IL-6 (ThermoFisher Scientific, # 88-7066-22) and TNF (ThermoFisher Scientific, # 88-7346-22).

Single-cell Ca^{2+} imaging, live-cell epifluorescence or TIRF microscopy and confocal microscopy.

THP1 and Jurkat T cells were loaded at 1×10^6 cells/ml with 1 μM Fura 2-AM for 40 min at 25ºC and attached to poly-L-lysine–coated coverslips. MEFs or BMDMs were grown overnight on coverslips and loaded with 1 μM Fura 2-AM for 40 min at 25ºC for imaging. Intracellular $[Ca^{2+}]_i$ measurements were performed using essentially the same methods as previously described[40]. For live-cell epifluorescence imaging of STING-GFP translocation kinetics, MEFs grown on coverslips were perfused with Ringer's solution containing (in mM): 155 NaCl, 4.5 KCl, 2 $CaCl_2$, 1 $MgCl_2$, 10 D-glucose, and 5 Na-HEPES (pH 7.4) and used for time course imaging. Cells were perfused with digitonin permeabilization buffer (50 mM HEPES, 100 mM KCl, 3 mM $MgCl_2$, 0.1 mM DTT, 85 mM sucrose, 0.2% BSA, 1 mM ATP, 0.1 mM GTP, pH 7.0) containing 1 μM 2',3'-cGAMP for 10 mins and then the medium was replaced with Ringer's solution. For TIRF analysis of STIM1-YFP translocation, MEFs were plated onto coverslip bottom dishes in medium and used for experiments. Medium was replaced with Ringer's solution and cells were treated with 1 μM thapsigargin for passive depletion of ER Ca^{2+} stores to monitor STIM1 translocation. TIRF microscopy was performed using an Olympus IX2 illumination system mounted on an Olympus IX51 inverted microscope using previously described methods[37]. Acquisition and image analysis were performed using Slidebook (Intelligent Imaging Innovations, Inc.) software and graphs

were plotted using OriginPro8.5 (Originlab). For quantification of TIRF intensity across different cells, individual regions of interest were selected and data were analyzed as the ratio of fluorescence intensity at each time-point (F) to that at the start of the experiment (F_0). For confocal analysis, uninfected or HSV-infected MEFs were fixed for 20 mins with 2.5% PFA at room temperature, permeabilized in buffer containing PBS + 0.2% Triton X-100, blocked with same buffer containing 1% BSA and used for staining of ERGIC marker and confocal analysis. Confocal laser scanning microscopy was performed using Fluoview FV10i Confocal Microscope (Olympus), images were captured with a 60x oil objective. Images were processed for enhancement of brightness or contrast using Fluoview software.

Generation of STIM1, STIM2 and STING-deficient cells using CRISPR-Cas9 system.

To generate lentiviruses for transduction, HEK293T cells were transfected with plasmid(s) encoding sgRNA and packaging vectors (pMD2.G and psPAX2, Addgene) using calcium phosphate transfection method. Lentiviruses encoding Cas9 were generated using the same technique. Culture supernatants were harvested at 48 and 72 hours post transfection and used for infection (50% of Cas9-encoding virus + 50% of sgRNA-encoding virus) of MEFs, THP1 or Jurkat T cells together with polybrene (8 μg/ml) using the spin-infection method. Cells were selected with puromycin (1 μg/ml) and blasticidin (5 μg/ml) 48 hours post infection. The sequences of the sgRNAs are described in Supplementary Table 1.

Immunoprecipitation and immunoblotting.

For immunoprecipitation, cDNA encoding full-length or fragments (a.a. 1–154 and 149–379) of FLAG-tagged STING and 6xHis-tagged STIM1 was transfected into HEK293T cells. Transfected cells (2×10^7) were lysed in lysis buffer (20 mM Tris-Cl, 2 mM EDTA, 135 mM NaCl, 10% (vol/vol) glycerol, 0.5% Igepal CA-630, protease inhibitor mixture, pH 7.5) and centrifuged at 100,000 x g for 1 hour before preclearing with protein G-Sepharose. Lysates were immunoprecipitated with anti-FLAG antibody-conjugated resin for 6 hours. Immunoprecipitates were washed five times in lysis buffer and analyzed by immunoblotting. For immunoblot analyses, cells were lysed in RIPA buffer (10 mM Tris-Cl, 1% Triton X-100, 0.1% SDS, 140 mM NaCl, 1 mM EDTA, 0.1% sodium deoxycholate, and cOmplete Protease Inhibitor Cocktail [Sigma-Aldrich], pH 8.0) and centrifuged to remove debris. Samples were separated on 8–10% SDS-PAGE. Proteins were transferred to nitrocellulose membranes and subsequently analyzed by immunoblotting with relevant antibodies. For dithiobis succinimidyl propionate (DSP) crosslinking, MEFs or HEK293T cells were left untreated or treated with 0.125, 0.25, 0.5, or 1.0 mM of DSP for 1 hour on ice, followed by quenching with 20 mM Tris-Cl, pH 7.5. Cells were lysed in SDS loading dye under non-reducing conditions (without β-Mercaptoethanol) and separated on 10% SDS-PAGE and immunoblotted for detection of indicated proteins. For endogenous immunoprecipitation, HEK293 cells were lysed in lysis buffer (same as above) and centrifuged at 100,000 x g for 1 hour before preclearing with protein G-Sepharose. Lysates were incubated with 2 μg of anti-STING antibody (Cell Signaling Technologies) overnight and subsequently with protein G-Sepharose for 2 hours. For immunoprecipitation of STING SAVI mutants with endogenous STIM1, HEK293T stably expressing FLAG-tagged human $STING^{WT}$, $STING^{V147M}$, $STING^{N154S}$ or $STING^{V155M}$ cDNAs were lysed in lysis buffer (same as

above), centrifuged at 100,000 x g for 1 hour, pre-cleared and incubated with anti-FLAG antibody-conjugated resin overnight in lysis buffer containing 0.1% Igepal CA-630 and processed as described above. PBMCs were lysed in NP40 Lysis Buffer (VWR Life Science) containing cOmplete Protease Inhibitor Cocktail (Sigma-Aldrich) and centrifuged to remove debris. 20 μg of total protein from healthy control or patient samples was separated on a 4–12% Bis-Tris Plus Gel (ThermoFisher), transferred to polyvinylidene difluoride (PVDF) membrane and subsequently analyzed by immunoblotting with relevant antibodies.

Purification of recombinant proteins from *E. coli*.

Full-length and fragments (a.a. 1–249, 250–400, 324–448, 400–600, and 600–685) of STIM1 were subcloned into pGEX4T-1 plasmid. GST fusion protein expressing transformants were grown in liquid cultures and induced with isopropyl-1-thio-β-D-galactopyranoside (IPTG, 0.2 mM) at 18°C overnight. Subsequently, cells were harvested and resuspended in lysis buffer (50 mM NaH_2PO_4, 500 mM NaCl, 10% glycerol, pH 8.0) containing protease inhibitors and 0.5% Triton X-100. Lysates were sonicated, centrifuged to remove debris and incubated with glutathione sepharose 4B beads for 2 hrs. After washing 8 times with lysis buffer, the beads were stored in lysis buffer without Triton X-100 at −20˚C.

GST pulldown analysis.

cDNA encoding full-length and fragments of STING-FLAG was transfected into HEK293T cells. Transfected cells (2×10^7) were lysed in lysis buffer (20 mM Tris-Cl, 2 mM EDTA, 135 mM NaCl, 10% (vol/vol) glycerol, 0.5% Igepal CA-630, protease inhibitor mixture, pH 7.5) and centrifuged at 100,000 x g for 1 hour before preclearing with protein G-Sepharose. Lysates were incubated with 20 μg of GST or GST-tagged fragments of STIM1 for 18 hours in binding buffer (0.5% Igepal CA-630, 20 mM Tris-HCl, 100 mM NaCl, 2 mM EDTA, 10% glycerol, protease inhibitors, pH 7.5). Pulldown samples were washed five times with lysis buffer and analyzed by immunoblotting for indicated proteins.

HSV infection in mice.

Age and gender-matched control (*Stim1*$^{fl/fl}$ or *Orai1*$^{fl/fl}$), *Stim1*$^{fl/fl}$*Lyz2*-cre or *Orai1*$^{fl/fl}$*Lyz2*-cre mice were intravenously injected with 1×10^7 pfu of HSV-1 17+ strain. The viability of the infected mice was monitored for 10 days. Mouse serum was collected at indicated times after infection for measurement of serum cytokine by ELISA.

Statistical analysis.

Statistical analysis was performed using the Origin2018b software (OriginLab, Northampton, MA, USA). Data are presented as mean ± s.e.m. For all dataset, normality and homogeneity of variance were evaluated by Shapiro-Wilk test and Levene test respectively, to ensure that the assumptions inherent to parametric significance testing were not violated. Statistical significance to compare two quantitative groups was evaluated using two-tailed/unpaired t-test. When multiple groups and/or multiple condition comparisons were necessary, one-way or two-way ANOVA was performed followed by a Tukey HSD post-hoc

test. Statistical comparison of multiple counts in contingency tables was performed using Chi-square test followed by pairwise analysis of differences as post-hoc test. A critical value for significance of $P < 0.05$ was used throughout the study, and statistical thresholds of 0.05, 0.005 as well as 0.0005 are indicated in the figures by asterisks (see legends for details).

Supplementary Material

Refer to Web version on PubMed Central for supplementary material.

ACKNOWLEDGEMENTS

We thank S. Bensinger (UCLA) for sharing THP1 cells, X. Liu and S. Smale (UCLA) for BMDM differentiation protocols and reagents. We thank N-H. Park, K-H. Shin, M. K. Kang, R. Kim, Y. Wang and T. M. Vondriska for sharing their confocal imaging facilities. We thank J-L. Casanova (Rockefeller University) for providing STIM1 patient B cell line. This work was supported by the National Institute of Health grants AI083432 and DE028432 (Y.G.) and AI130653 (S.S.). This work was also supported in part by CA180779, CA200422, AI073099, AI116585, AI129496, AI140705, DE023926, DE027888, Fletcher Jones Foundation, and Whittier Foundation (J.U.J.).

References

1. Ishikawa H & Barber GN STING is an endoplasmic reticulum adaptor that facilitates innate immune signalling. Nature 455, 674–678 (2008). [PubMed: 18724357]
2. Zhong B et al. The adaptor protein MITA links virus-sensing receptors to IRF3 transcription factor activation. Immunity 29, 538–550 (2008). [PubMed: 18818105]
3. Sun W et al. ERIS, an endoplasmic reticulum IFN stimulator, activates innate immune signaling through dimerization. Proc Natl Acad Sci U S A 106, 8653–8658 (2009). [PubMed: 19433799]
4. Barber GN STING: infection, inflammation and cancer. Nat Rev Immunol 15, 760–770 (2015). [PubMed: 26603901]
5. Chen Q, Sun L & Chen ZJ Regulation and function of the cGAS-STING pathway of cytosolic DNA sensing. Nat Immunol 17, 1142–1149 (2016). [PubMed: 27648547]
6. Li T & Chen ZJ The cGAS-cGAMP-STING pathway connects DNA damage to inflammation, senescence, and cancer. J Exp Med (2018).
7. Li Y, Wilson HL & Kiss-Toth E Regulating STING in health and disease. J Inflamm (Lond) 14, 11 (2017). [PubMed: 28596706]
8. Yan N, Regalado-Magdos AD, Stiggelbout B, Lee-Kirsch MA & Lieberman J The cytosolic exonuclease TREX1 inhibits the innate immune response to human immunodeficiency virus type 1. Nat Immunol 11, 1005–1013 (2010). [PubMed: 20871604]
9. Ahn J, Gutman D, Saijo S & Barber GN STING manifests self DNA-dependent inflammatory disease. Proc Natl Acad Sci U S A 109, 19386–19391 (2012). [PubMed: 23132945]
10. Crow YJ & Manel N Aicardi-Goutieres syndrome and the type I interferonopathies. Nat Rev Immunol 15, 429–440 (2015). [PubMed: 26052098]
11. Liu Y et al. Activated STING in a vascular and pulmonary syndrome. N Engl J Med 371, 507–518 (2014). [PubMed: 25029335]
12. Melki I et al. Disease-associated mutations identify a novel region in human STING necessary for the control of type I interferon signaling. J Allergy Clin Immunol 140, 543–552 e545 (2017). [PubMed: 28087229]
13. Jeremiah N et al. Inherited STING-activating mutation underlies a familial inflammatory syndrome with lupus-like manifestations. J Clin Invest 124, 5516–5520 (2014). [PubMed: 25401470]
14. Dobbs N et al. STING Activation by Translocation from the ER Is Associated with Infection and Autoinflammatory Disease. Cell Host Microbe 18, 157–168 (2015). [PubMed: 26235147]
15. Zhang X et al. Cyclic GMP-AMP containing mixed phosphodiester linkages is an endogenous high-affinity ligand for STING. Mol Cell 51, 226–235 (2013). [PubMed: 23747010]

16. Prakriya M & Lewis RS Store-Operated Calcium Channels. Physiol Rev 95, 1383–1436 (2015). [PubMed: 26400989]
17. Feske S, Skolnik EY & Prakriya M Ion channels and transporters in lymphocyte function and immunity. Nat Rev Immunol 12, 532–547 (2012). [PubMed: 22699833]
18. Baba Y & Kurosaki T Role of Calcium Signaling in B Cell Activation and Biology. Curr Top Microbiol Immunol 393, 143–174 (2016). [PubMed: 26369772]
19. Srikanth S, Woo JS, Sun Z & Gwack Y Immunological Disorders: Regulation of Ca(2+) Signaling in T Lymphocytes. Adv Exp Med Biol 993, 397–424 (2017). [PubMed: 28900926]
20. Lacruz RS & Feske S Diseases caused by mutations in ORAI1 and STIM1. Ann N Y Acad Sci 1356, 45–79 (2015). [PubMed: 26469693]
21. Notarangelo LD, Kim MS, Walter JE & Lee YN Human RAG mutations: biochemistry and clinical implications. Nat Rev Immunol 16, 234–246 (2016). [PubMed: 26996199]
22. Brandman O, Liou J, Park WS & Meyer T STIM2 is a feedback regulator that stabilizes basal cytosolic and endoplasmic reticulum Ca2+ levels. Cell 131, 1327–1339 (2007). [PubMed: 18160041]
23. Soboloff J, Rothberg BS, Madesh M & Gill DL STIM proteins: dynamic calcium signal transducers. Nat Rev Mol Cell Biol 13, 549–565 (2012). [PubMed: 22914293]
24. Picard C et al. STIM1 mutation associated with a syndrome of immunodeficiency and autoimmunity. N Engl J Med 360, 1971–1980 (2009). [PubMed: 19420366]
25. Rice A et al. A report of novel STIM1 deficiency and 6 year follow up of two previous cases associated with mild immunological phenotype 10.31219/osf.io/4duxt (2018).
26. Guo H et al. NLRX1 Sequesters STING to Negatively Regulate the Interferon Response, Thereby Facilitating the Replication of HIV-1 and DNA Viruses. Cell Host Microbe 19, 515–528 (2016). [PubMed: 27078069]
27. Saitoh T et al. Atg9a controls dsDNA-driven dynamic translocation of STING and the innate immune response. Proc Natl Acad Sci U S A 106, 20842–20846 (2009). [PubMed: 19926846]
28. Lau L, Gray EE, Brunette RL & Stetson DB DNA tumor virus oncogenes antagonize the cGAS-STING DNA-sensing pathway. Science 350, 568–571 (2015). [PubMed: 26405230]
29. Yuan JP et al. SOAR and the polybasic STIM1 domains gate and regulate Orai channels. Nat Cell Biol 11, 337–343 (2009). [PubMed: 19182790]
30. Ishikawa H, Ma Z & Barber GN STING regulates intracellular DNA-mediated, type I interferon-dependent innate immunity. Nature 461, 788–792 (2009). [PubMed: 19776740]
31. Mukai K et al. Activation of STING requires palmitoylation at the Golgi. Nat Commun 7, 11932 (2016). [PubMed: 27324217]
32. Ouyang S et al. Structural analysis of the STING adaptor protein reveals a hydrophobic dimer interface and mode of cyclic di-GMP binding. Immunity 36, 1073–1086 (2012). [PubMed: 22579474]
33. Gao D et al. Cyclic GMP-AMP synthase is an innate immune sensor of HIV and other retroviruses. Science 341, 903–906 (2013). [PubMed: 23929945]
34. Cheshenko N et al. Herpes simplex virus triggers activation of calcium-signaling pathways. J Cell Biol 163, 283–293 (2003). [PubMed: 14568989]
35. Zhong B et al. The ubiquitin ligase RNF5 regulates antiviral responses by mediating degradation of the adaptor protein MITA. Immunity 30, 397–407 (2009). [PubMed: 19285439]
36. Wang Y et al. TRIM30alpha Is a Negative-Feedback Regulator of the Intracellular DNA and DNA Virus-Triggered Response by Targeting STING. PLoS Pathog 11, e1005012 (2015). [PubMed: 26114947]
37. Srikanth S et al. A novel EF-hand protein, CRACR2A, is a cytosolic Ca2+ sensor that stabilizes CRAC channels in T cells. Nat Cell Biol 12, 436–446 (2010). [PubMed: 20418871]
38. Gwack Y et al. Hair loss and defective T- and B-cell function in mice lacking ORAI1. Mol Cell Biol 28, 5209–5222 (2008). [PubMed: 18591248]
39. Stetson DB & Medzhitov R Recognition of cytosolic DNA activates an IRF3-dependent innate immune response. Immunity 24, 93–103 (2006). [PubMed: 16413926]

40. Srikanth S, Jung HJ, Ribalet B & Gwack Y The intracellular loop of Orai1 plays a central role in fast inactivation of Ca2+ release-activated Ca2+ channels. J Biol Chem 285, 5066–5075 (2010). [PubMed: 20007711]

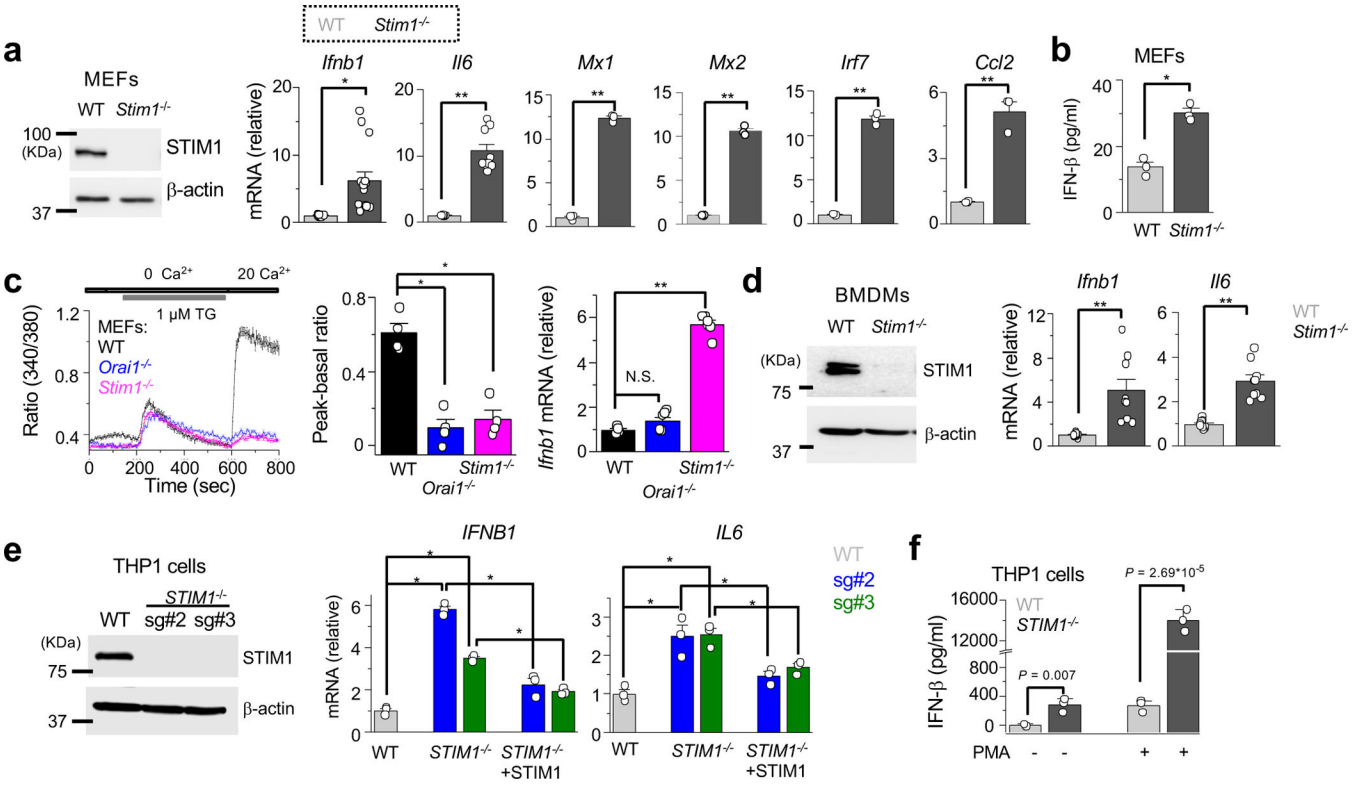

Figure 1. STIM1 deficiency spontaneously induces type I IFN response in murine and human cells.

a, Representative immunoblot showing expression of STIM1 in wild type (WT) and *Stim1*$^{-/-}$ MEFs (left). qPCR analysis of indicated cytokines and ISGs in unstimulated indicated MEFs (right). qPCR data show pooled technical replicates from two independent experiments (*Ifnb1* and *Il6*) and one representative triplicate from two independent experiments (other genes). **b**, Levels of secreted IFN-β from culture supernatants of unstimulated WT or *Stim1*$^{-/-}$ MEFs. **c**, Representative traces showing averaged SOCE from WT (31 cells), *Orai1*$^{-/-}$ (30 cells) and *Stim1*$^{-/-}$ (29 cells) MEFs after passive depletion of intracellular Ca^{2+} stores with 1 μM thapsigargin (TG) in the presence of external solution containing 20 mM Ca^{2+} (left). Bar graph (middle) shows averaged baseline subtracted SOCE (± s.e.m.) from four independent experiments. right: qPCR analysis of *Ifnb1* mRNA in indicated MEFs. **d**, Representative immunoblot showing expression of STIM1 in BMDMs (left). qPCR analysis of *Ifnb1* and *Il6* mRNA in unstimulated WT and *Stim1*$^{-/-}$ BMDMs (right). **e**, Immunoblot showing expression of STIM1 in wild type (WT) and *STIM1*$^{-/-}$ THP1 cells generated using two independent sgRNAs (sg#2) and 3 (sg#3). qPCR analysis of *IFNB1* and *IL6* mRNA in unstimulated WT, *STIM1*$^{-/-}$ THP1 cells and those reconstituted for expression of STIM1 (right two panels). **f**, Secreted IFN-β levels from culture supernatants of untreated or PMA-differentiated WT or *STIM1*$^{-/-}$ THP1 cells. Data show representative triplicate from two independent experiments (panels **b, e** and **f**) or pooled technical replicates from two (**c**) or three (**d**) independent experiments. All immunoblot data (panels **a**, **d** and **e**) are representative of three independent experiments with similar results. Data are shown as mean ± s.e.m. *p < 0.005, and **p < 0.0005 (unpaired/two-tailed *t* test – a, b, d; One-way ANOVA – c; and Two-way ANOVA – e).

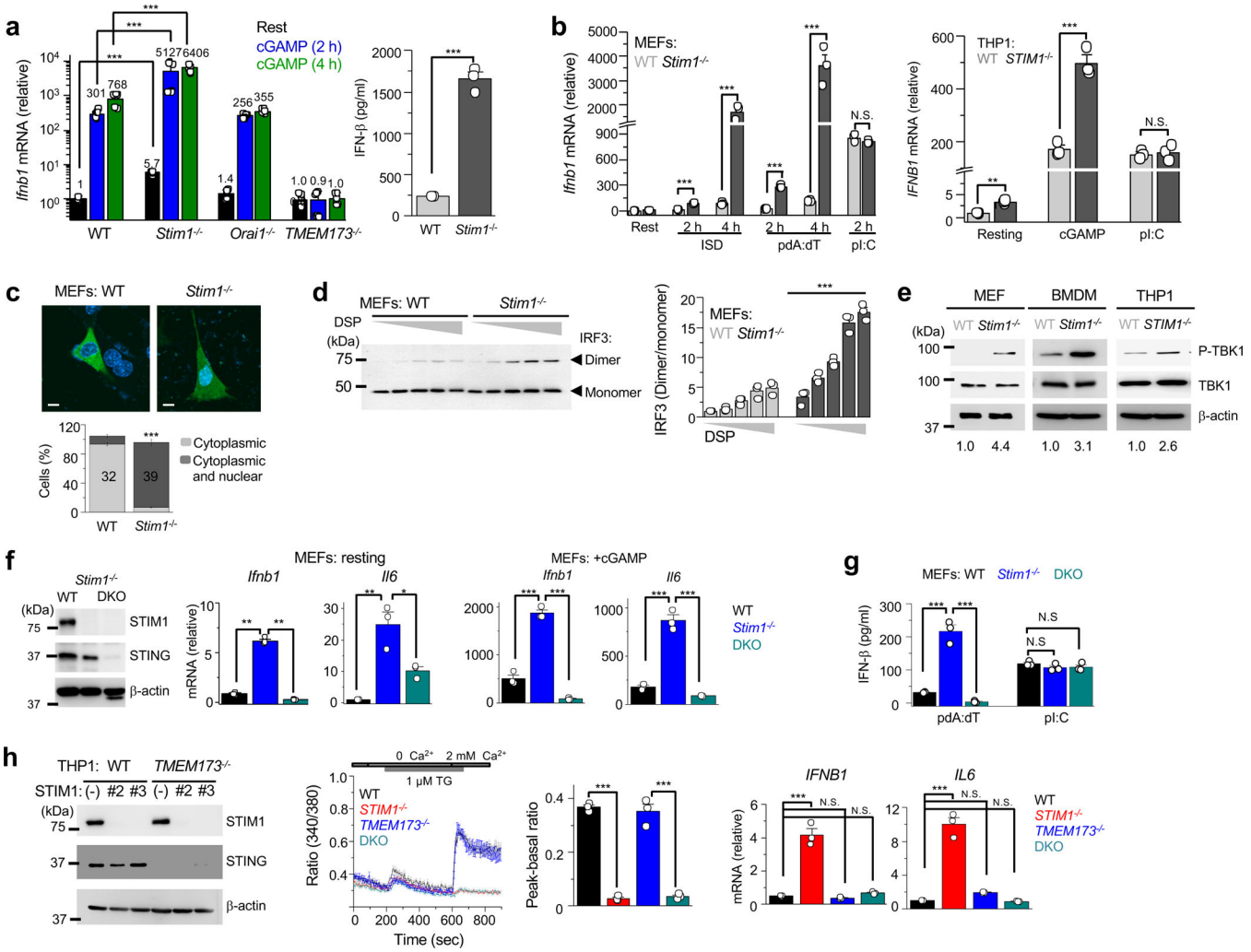

Figure 2. STING-TBK1-IRF3 pathway links loss of STIM1 expression to *Ifnb1* transcription.

a, qPCR analysis of *Ifnb1* mRNA in indicated MEFs under resting conditions or after stimulation with 2',3'-cGAMP for 2 or 4 h (left). Numbers on top indicate average fold change relative to WT MEFs. Secreted IFN-β levels from culture supernatants of indicated MEFs after stimulation with 2',3'-cGAMP (right). Data show pooled technical replicates from two independent experiments (qPCR) or one representative triplicate from two independent experiments (ELISA) with similar results. **b**, qPCR analysis of *Ifnb1* transcripts in indicated MEFs transfected with interferon stimulatory DNA (ISD), poly(dA:dT) or poly (I:C) for indicated time (left). qPCR analysis of *IFNB1* mRNA from untreated or indicated nucleic acid-transfected THP1 cells. **c**, Representative confocal images showing localization of GFP-IRF3 in indicated MEFs. Bar graph below depicts quantification from indicated number of cells. Scale bars, 5 μm. **d**, Representative immunoblot for detection of IRF3 under non-reducing conditions in DSP-crosslinked indicated MEFs, (left). Bar graph (right) shows densitometry analysis of IRF3 ratio (dimer/monomer) from three independent experiments. **e**, Representative immunoblots showing expression of phospho-TBK1 (P-TBK1), total TBK1, and *β*-actin from indicated cells. Numbers below indicate normalized fold change in ratio of P-TBK1/total TBK1. **f**, Representative immunoblots showing expression of STIM1

and STING in WT, *Stim1*$^{-/-}$, or *Stim1*$^{-/-}$ and *Tmem173*$^{-/-}$ double knock out (DKO) MEFs (left). Expression of *Ifnb1* and *Il6* transcripts in indicated MEFs under resting conditions (left two panels) or 4 h after stimulation with 2',3'-cGAMP (right two panels). **g**, Secreted IFN-β levels from culture supernatants of indicated MEFs after stimulation with indicated nucleic acids. **h**, Representative immunoblots showing expression of STIM1 and STING in WT, *STIM1*$^{-/-}$, *TMEM173*$^{-/-}$ or *STIM1*$^{-/-}$ and *TMEM173*$^{-/-}$ double knock out (DKO) THP1 cells (left). Representative traces of averaged SOCE from WT (33 cells), *STIM1*$^{-/-}$, (30 cells), *TMEM173*$^{-/-}$ (31 cells) and DKO (31 cells) THP1 cells after passive depletion of intracellular Ca^{2+} stores with 1 μM thapsigargin (TG) in the presence of external solution containing 2 mM Ca^{2+} (middle). Bar graph shows averaged baseline subtracted SOCE (± s.e.m.) from three independent experiments. Right panels show qPCR analysis of *IFNB1* or *IL6* mRNA in indicated THP1 cells. Data show representative triplicates from two independent experiments with similar results (**b**, **d**, **f**, **g** and **h**) unless indicated. All immunoblots are representative of at least three independent experiments with similar results. Data are shown as mean ± s.e.m. *p < 0.05, **p < 0.005, ***p < 0.0005 [Two-way ANOVA – a (left panel); unpaired/two-tailed *t* test – a (right panel), b; Chi-square test – c; and One-way ANOVA – d, f, g, h].

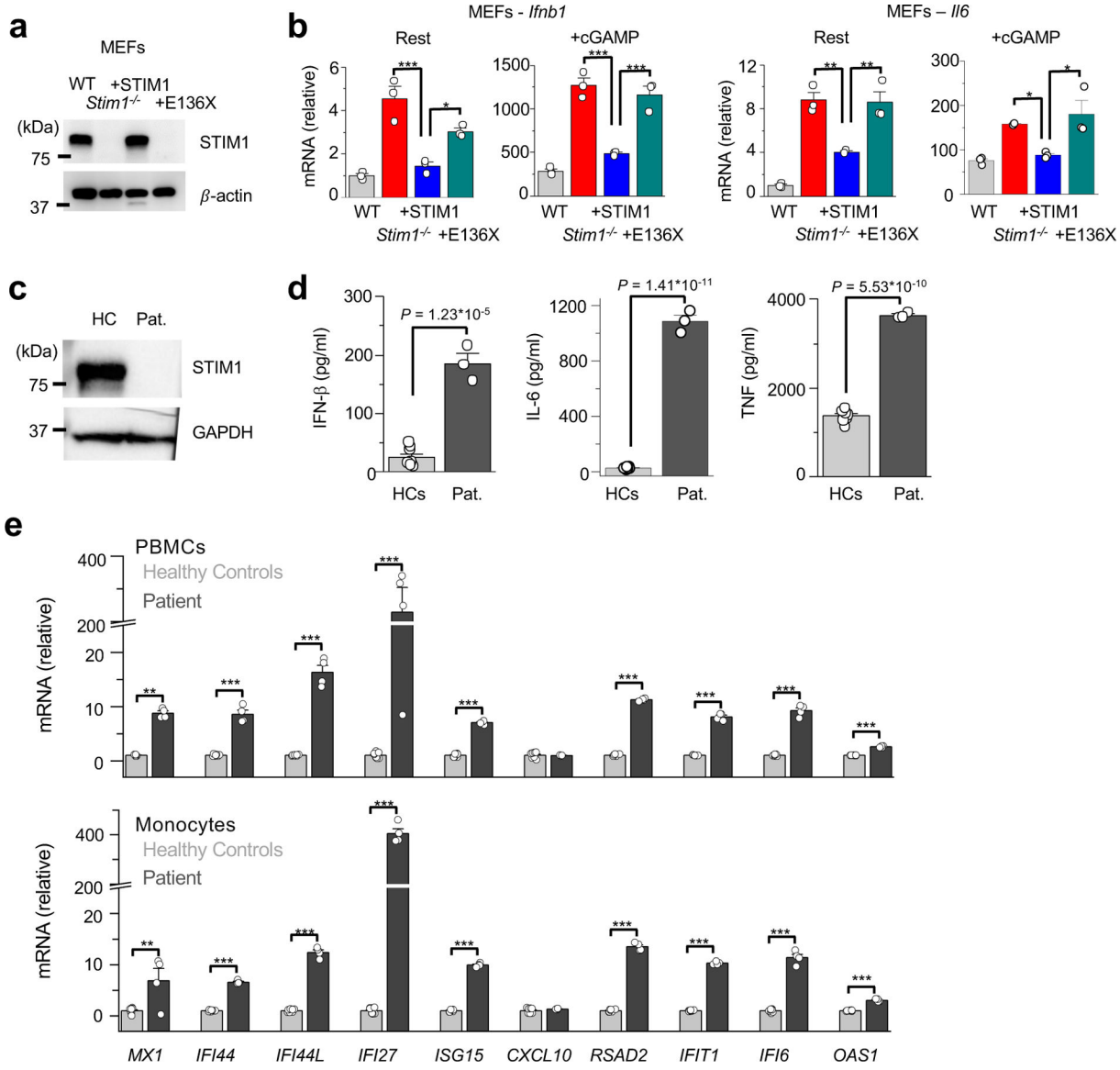

Figure 3. STIM1 deficiency causes enhanced type I IFN response in patient cells.

a, Representative immunoblot showing expression of STIM1 in WT, *Stim1*$^{-/-}$ MEFs or those expressing either WT STIM1 (+STIM1) or STIM1^{E136X} (+E136X) mutant. **b**, qPCR analysis of *Ifnb1* and *Il6* mRNA in indicated MEFs under resting conditions or 2 h after stimulation with 2',3'-cGAMP. Data show representative triplicate from two independent experiments. **c**, Representative immunoblot showing expression of STIM1 and GAPDH in PBMCs isolated from a healthy control (HC) and patient (Pat.). **d**, Levels of indicated cytokines in serum samples from healthy controls (three independent donors) and STIM1-deficient patient. Data show one representative triplicate from two independent experiments (n=9 for three HCs). **e**, Taqman qPCR analysis of indicated ISGs from peripheral blood mononuclear cells (PBMCs, top) or purified monocytes (below) from two independent healthy controls and STIM1-deficient patient. Patient data (normalized to those of healthy controls) are derived from two independent experiments performed in duplicates. Data are

shown as mean ± s.e.m. *p < 0.05, **p < 0.005, ***p < 0.0005 (One-way ANOVA – b; and unpaired/two-tailed *t* test – d, e).

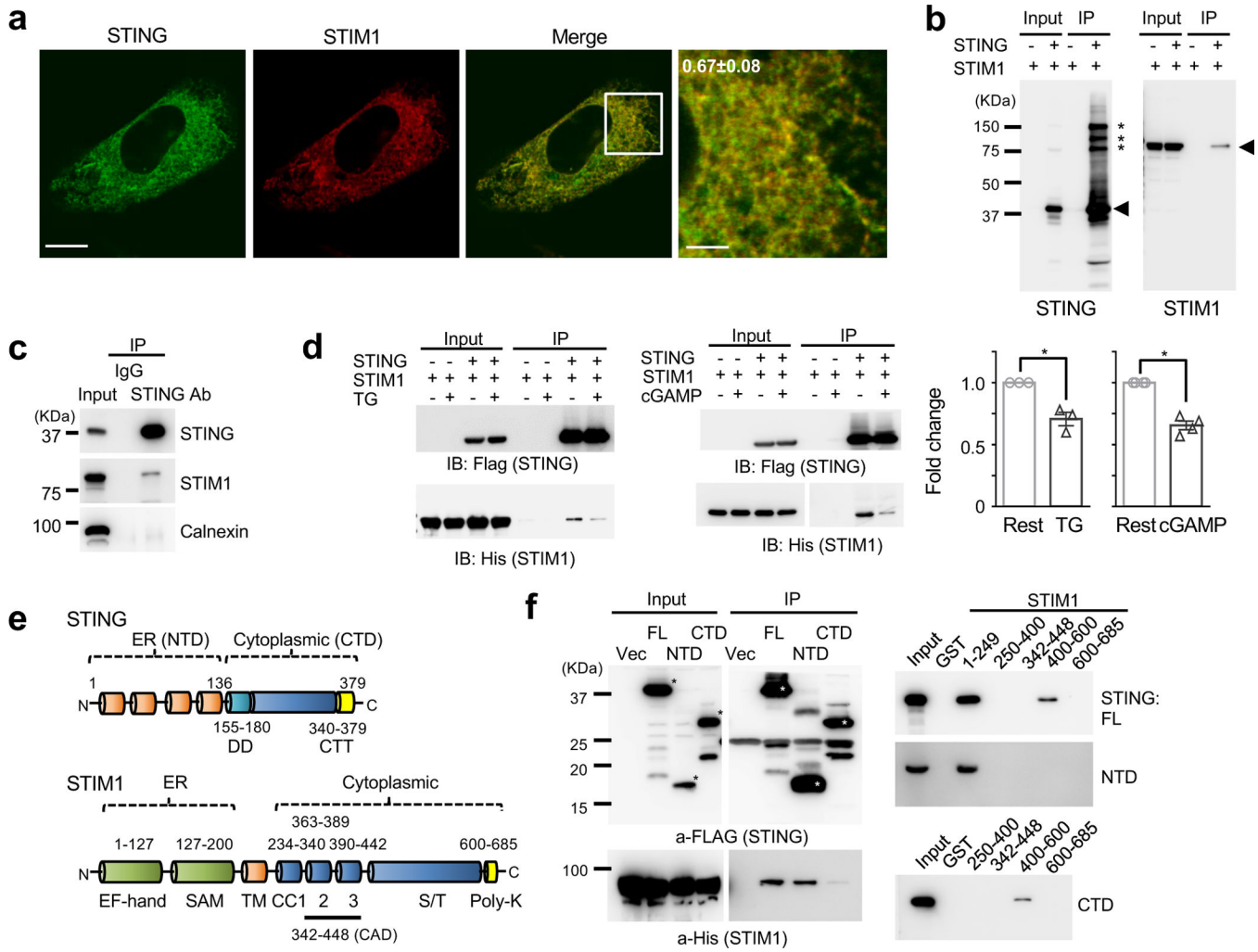

Figure 4. STIM1 interacts with STING for its retention in the endoplasmic reticulum.

a, Representative confocal microscopy image of STING-GFP and STIM1 in a MEF cell. Scale bar, 5 μm, Inset – 1 μm. Pearson's r = 0.67 ± 0.08 from 9 cells. **b**, FLAG-immunoprecipitates (IP) from lysates of HEK293T cells overexpressing FLAG-tagged STING and His-tagged STIM1 were immunoblotted for detection of STIM1. Arrow, monomeric STING or STIM1; *, STING multimers. **c**, Immunoprecipitates of endogenous STING from HEK293 cells were immunoblotted for detection of indicated proteins. **d**, FLAG-immunoprecipitates (IP) from lysates of HEK293T cells expressing FLAG-tagged STING and His-tagged STIM1 with or without treatment with thapsigargin (1 μM, 10 min; left) or 2', 3'-cGAMP (1 μM, 30 min and further incubation in media for 1 h) were immunoblotted for detection of the indicated proteins. Bar graphs show densitometry analysis of normalized fold changes (mean ± s.e.m.) in STIM1 and STING band intensity from three (left) and four (right) independent experiments. **e**, Schematic showing domain structure of STING and STIM1 as indicated in the text. Amino acid residues of STING and STIM1 fragments used in this study are indicated. **f**, Left – FLAG-immunoprecipitates (IP) from lysates of HEK293T cells expressing FLAG-tagged full-length STING (FL), NTD (a.a. 1–140), and CTD (a.a. 140–379) were immunoblotted for detection of STIM1. Right –

Purified recombinant GST-fused indicated fragments of STIM1 incubated with lysates of HEK293T cells expressing FLAG-tagged, FL, NTD or CTD of STING were immunoblotted with anti-FLAG antibody. Immunoblots in panels **b**, **c**, and **f** are representative of four independent experiments. *$p < 0.005$ (unpaired/two-tailed *t* test - d).

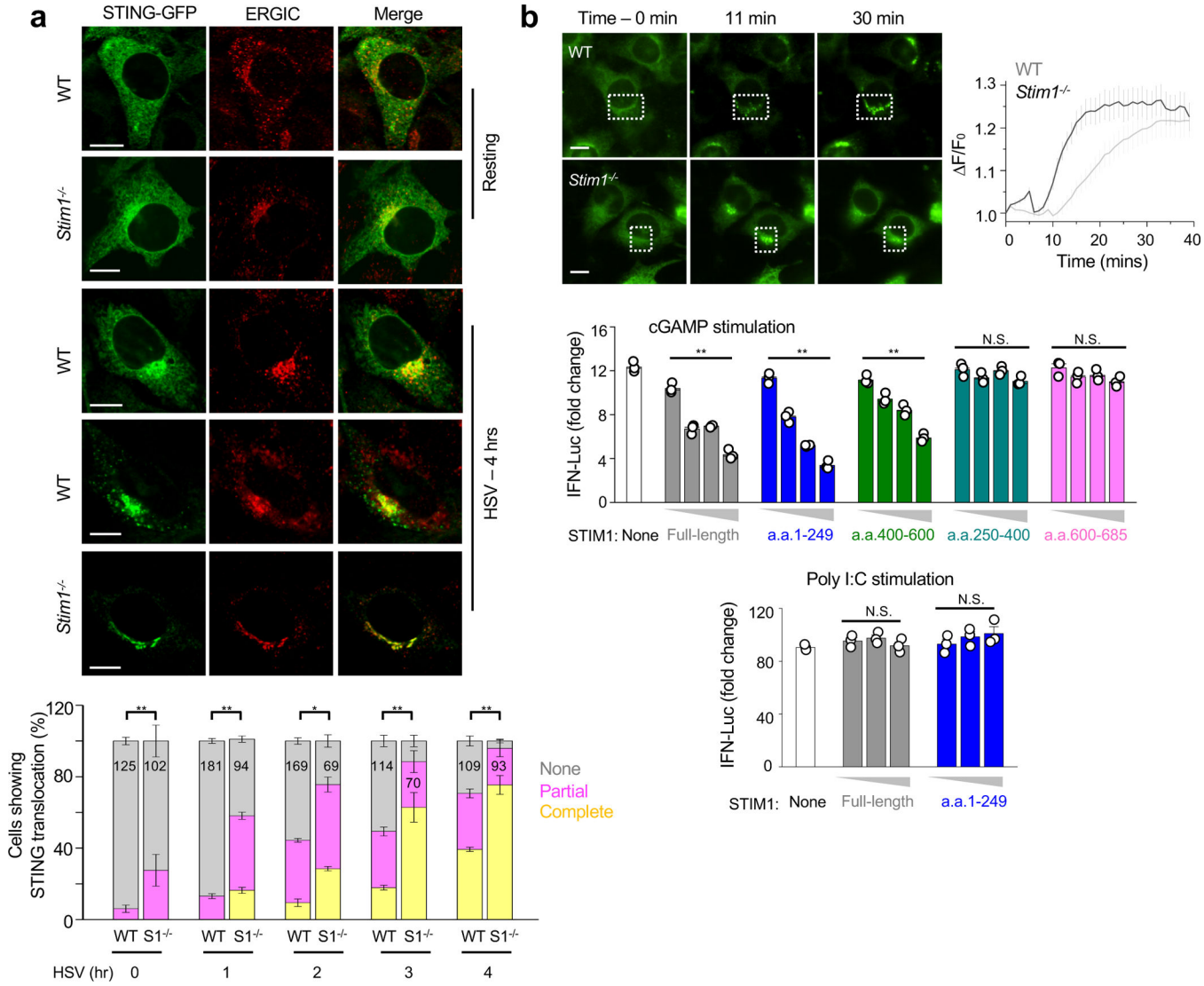

Figure 5. STIM1 inhibits STING trafficking to the ER-Golgi intermediate compartment.

a, Representative confocal microscopy images of WT or *Stim1*$^{-/-}$ MEFs stably expressing STING-GFP under resting conditions (top two panels) or 4 h after HSV-1 infection (bottom 3 panels) and stained for endogenous p58 (ERGIC). Scale bars, 10 μm. Bar graph shows quantification of indicated number of cells showing STING translocation to the ERGIC under resting conditions or after infection with HSV-1 for indicated times. Data are derived from two independent experiments. **b**, Representative live cell epifluorescence images of WT (top) or *Stim1*$^{-/-}$ (bottom) MEFs after treatment with 1 μM 2', 3'-cGAMP for the indicated times showing translocation of STING-GFP into the ERGIC (left). Line graph on the right shows normalized rate of translocation of STING in WT (9 cells) and *Stim1*$^{-/-}$ (11 cells) MEFs from two independent experiments. Scale bar, 10 μm. **c,** Reporter assays for *Ifnb1* promoter activity in HEK293T cells transfected with STING and increasing amounts of full length STIM1 or its indicated fragments, 6 hours after stimulation with 2', 3' cGAMP (top) or poly(I:C) (below). Data show representative triplicate from two independent

experiments. *p < 0.005, **p < 0.0005 Chi square test (a) and one-way ANOVA (c); N.S. – not significant.

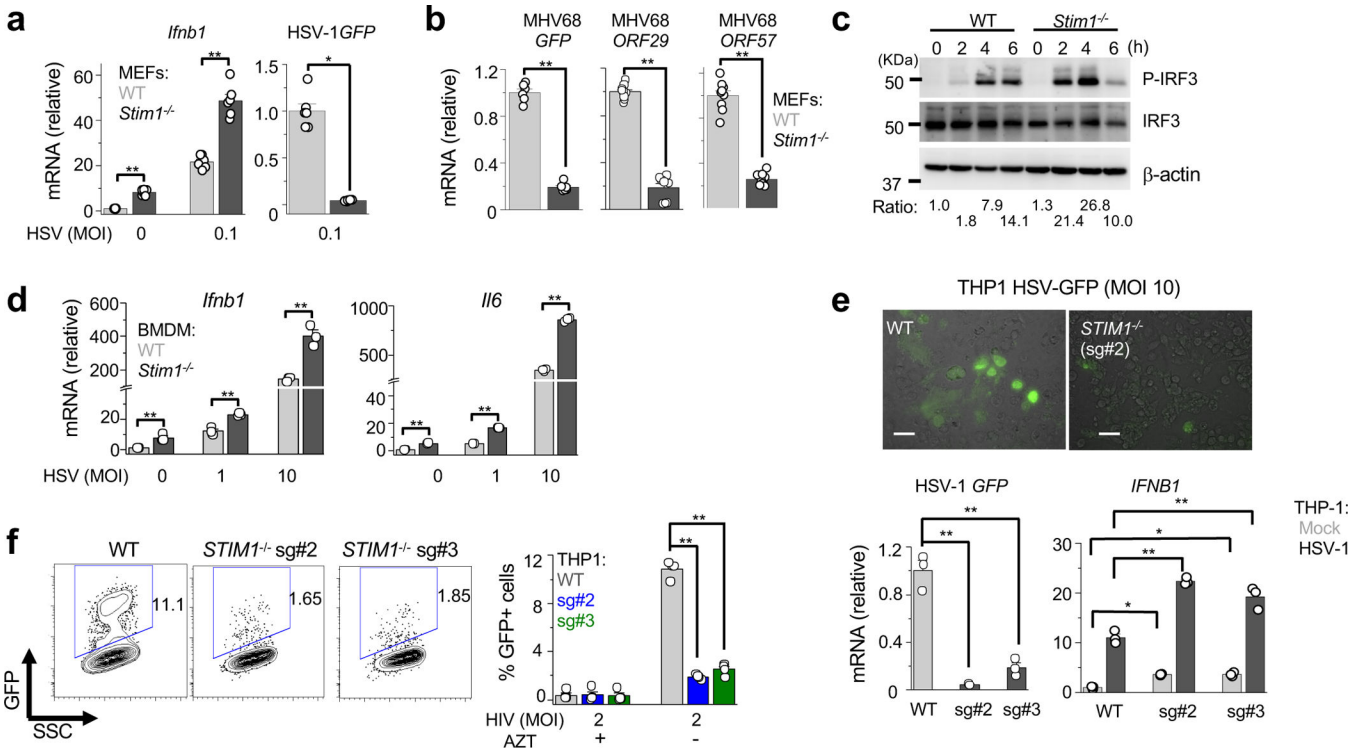

Figure 6. Ablation of STIM1 enhances host defense towards DNA viruses and HIV by priming type I IFN responses.

a, qPCR analysis of *Ifnb1* and GFP transcripts in uninfected or HSV-1-GFP-infected (MOI 0.1, 24 h) WT or *Stim1*$^{-/-}$ MEFs. Data show pooled technical replicates from two independent experiments. **b,** qPCR analysis of GFP and indicated viral mRNAs in MHV-68-GFP-infected (MOI 0.2, 24 h) WT or *Stim1*$^{-/-}$ MEFs. Data show pooled technical replicates from three independent experiments. **c**, Representative immunoblots showing expression of phospho-IRF3 (P-IRF3), total IRF3, and *β*-actin from untreated or HSV-1-infected (MOI 5.0) WT or *Stim1*$^{-/-}$ MEFs for indicated time points. **d**, qPCR analysis of *Ifnb1* and *Il6* mRNA in untreated or HSV-1-GFP-infected (indicated MOI, 24 h) WT or *Stim1*$^{-/-}$ BMDMs. Data shows representative triplicate from two independent experiments. **e**, Top two panels show representative GFP images in HSV-1-GFP-infected (MOI 10, 24 h) WT, (left) and *STIM1*$^{-/-}$ (right) THP-1 cells. Below: qPCR analysis of *IFNB1* and GFP transcripts from the same cells. Scale bars, 10 μm. Data shows representative triplicate from two independent experiments. **f**, Representative flow plots showing frequency of HIV-GFP-infected WT (left) or two different *STIM1*$^{-/-}$ (right two panels) THP1 cell lines (MOI 2.0, 24 h). Bar graph shows averaged frequency of HIV-GFP-positive indicated THP1 cell lines in the presence or absence of HIV reverse transcriptase inhibitor azidothymidine (AZT, 5 μM) from four independent experiments. Immunoblots in panel **c** and epifluorescence images in panel **e** are representative of three and two independent experiments respectively. *p < 0.005 and **p < 0.0005 [Two-way ANOVA – a (left panel), d, e (right panel), f; unpaired/two-tailed *t* test – a (right panel), b; One-way ANOVA – e (left panel)].

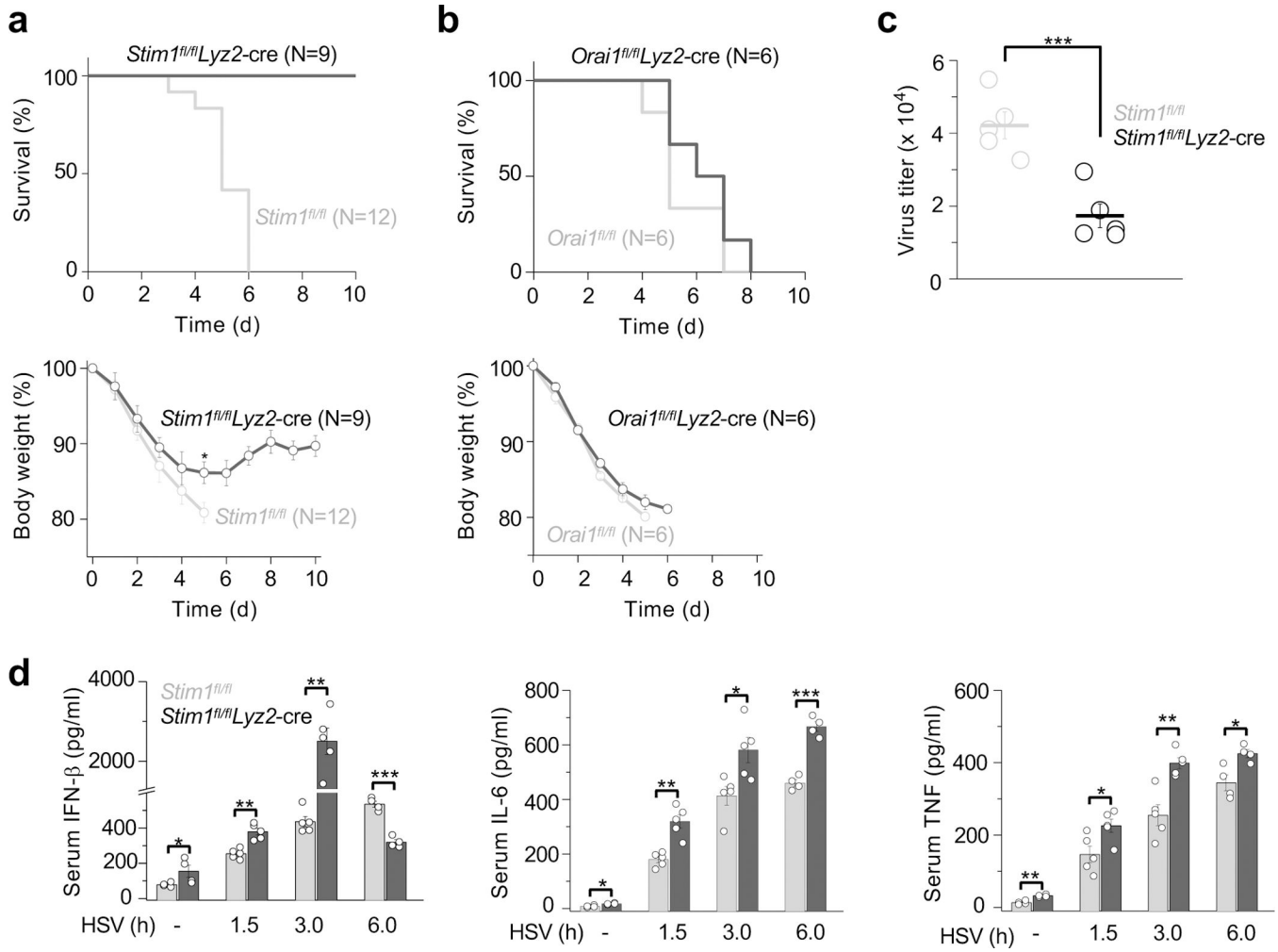

Figure 7. STIM1 deficiency enhances host defense against HSV-1 infection in vivo.

a, Kinetics of survival (top) and body weight changes (bottom) of indicated numbers of control (*Stim1*$^{fl/fl}$) and STIM1-deficient (*Stim1*$^{fl/fl}$*Lyz2*-cre) mice (6–7-week old) after intravenous injection with HSV-1 (1×10^7 PFU per mouse). **b**, Kinetics of survival (top) and body weight changes (bottom) of indicated numbers of control (*Orai1*$^{fl/fl}$) and Orai1-deficient (*Orai1*$^{fl/fl}$*Lyz2*-cre) mice after intravenous injection with HSV-1 (1×10^7 PFU per mouse). Mice that lost >20% body weight were euthanized. **c**, Virus load in control (*Stim1*$^{fl/fl}$) and STIM1-deficient (*Stim1*$^{fl/fl}$*Lyz2*-cre) mouse brains 3 days after intravenous injection with HSV-1. **d**, ELISA analyses of the indicated cytokines from the sera of control (*Stim1*$^{fl/fl}$) and *Stim1*-deficient (*Stim1*$^{fl/fl}$ *Lyz2*-cre) mice after intravenous injection with HSV-1 for indicated times. Data in panels **a** and **b** are pooled from two independent experiments. Panels **c** and **d** show mean +/− s.e.m. from indicated number of animals (each symbol represents data from individual animal). *p < 0.05, **p < 0.005, ***p < 0.0005 (unpaired/two-tailed *t* test).